

# EXPERIMENTAL AND NUMERICAL INVESTIGATION OF NOISE GENERATION IN HYDROGEN AND METHANE-HYDROGEN LAMINAR FLAMES

Francesco G. Schiavone<sup>1</sup>, Matthieu Durand<sup>2</sup>, Marco Torresi<sup>1</sup>, Sergio M. Camporeale<sup>1</sup>, Thierry Schuller<sup>2,3</sup> & Davide Laera<sup>1</sup>

<sup>1</sup>Department of Mechanics, Mathematics and Management, Polytechnic University of Bari, Via Orabona 4, Bari 70125, Italy

<sup>2</sup>Institut de Mécanique des Fluides de Toulouse, IMFT, Université de Toulouse, CNRS, Toulouse 31400, France <sup>3</sup>Institut Universitaire de France (IUF)

## **Abstract**

The direct combustion noise generation in hydrogen-air and methane-hydrogen-air laminar flames is investigated by means of experimental measurements and high-fidelity numerical simulations. Premixed M-shaped flames, stabilized over a cylindrical bluff-body burner at atmospheric conditions, are submitted to a weak acoustic perturbation, inducing oscillations of flame surface area and heat release rate, thus leading to noise emission. The similarities and differences in noise generation between the two fuel mixtures are investigated by comparing flames with either the same flame height or the same ratio between the flow velocity and laminar burning velocity. Under the conditions considered in this study, methane-hydrogen flames exhibit a more accentuated flame-flame interaction, and consequently a larger pressure fluctuation than hydrogen flames, even though the sound pressure levels are comparable for all cases. Moreover, the response of the hydrogen flames is in phase with the imposed acoustic excitation, while a delay is observed in the case of methane-hydrogen flames.

**Keywords:** hydrogen, laminar flames, premixed flames, combustion noise

# 1. Introduction

Aviation is a strongly carbon-emitting sector, with the current carbon dioxide (CO<sub>2</sub>) emissions estimated to be 1 gigatonne per year [1]. Given the expected increase in air traffic, with a projected doubling of air travel demand by 2040 according to the International Air Transport Association [2], these emissions are expected to considerably increase under scenarios of continued growth [1]. Radical changes are thus demanded from a technological point of view to reach the ambitious target of netzero carbon emissions by 2050 [3] in the context of an increasing demand. Hydrogen as a fuel is recognized as one of the most important candidates to reach the objective of a decarbonized aviation [4], especially for short-distance routes [5]. Hydrogen combustion for aviation applications has been studied for decades, with flight tests conducted in 1957 by the American National Advisory Committee for Aeronautics (NACA) using a Martin B57-B airplane [6], and in 1988 by the Soviet Tupolev Design Bureau with the Tu-155 aircraft, a modified version of the more famous Tu-154 [7]. Nevertheless, the characteristic physical-chemical properties of this fuel (e.g., wide flammability range, large burning velocity, small quenching distance, tendency to autoignition and differential diffusion) and the technological gap with conventional hydrocarbons pose obstacles to the industrial application of hydrogen combustion [8].

In parallel to pollutant emissions, ambitious targets have been set to reduce aircraft noise emissions too [9]. Indeed, aircraft noise is a matter of significant concern for the aviation industry, given the adverse impact on the quality of life, health, and property value of communities nearby airports and

main flight corridors [10]. Noise has short-term effects upon observers (e.g., annoyance, physiological change, and reduction in efficiency), and causes also long-term physiological impairment, such as hearing damage, speech, and sleep interference [11]. Over the last decades, technological developments such as the introduction of the turbofan engine, the increase in bypass ratio, and novel fan blade designs have led to a reduction of jet, fan and external aerodynamic noise, leaving combustion noise as a leading contributor to overall aircraft noise [10, 11].

Combustion noise can be distinguished into two components, direct and indirect [12]. Direct noise is associated to acoustic perturbations due to unsteady volumetric expansion and contraction in the reaction zone [13], and fluctuations of heat release rate [14]. This noise component is broadband, with random phase and peak frequencies below 500 Hz [15], and would occur even for combustion processes in unbounded space [11]. Indirect combustion noise, or entropy noise [16], is instead produced by the acceleration of a flow with non-uniform entropy or vorticity distributions [11].

Despite over six decades of research on sound emissions by combusting jet flows [17], there is still a lack of fundamental understanding on combustion noise generation mechanisms. Moreover, while noise generation has been extensively studied for hydrocarbon fuels [18], investigations involving hydrogen are fewer. Hydrogen flames are characterized by fast ignition, high burning velocities and fast diffusive transport (sub-unity Lewis number) promoting thermodiffusive instabilities [19]. Given the higher burning intensity, turbulent hydrogen flames have a shorter length compared to hydrocarbons' [20], leading to a shift of radiated noise to higher frequencies and making them more responsive to high-frequency incoming acoustic waves [21, 22]. Indeed, flame length is an essential feature as it controls the cutoff frequency of the flame transfer function [23] and the peak frequency of the broadband combustion noise radiated by unconfined flames [24]. Hydrogen flames also feature smaller flame structures, leading to a strong modification in the acoustic energy radiated. Furthermore, hydrogen preferential diffusion [25] enhances local composition and density non-homogeneities, consequently promoting noise generation mechanisms. Thermodiffusive effects, characteristic of very lean hydrogen flames, lead to significant flame front wrinkling and to the chaotic formation and destruction of cellular structures along the flame front [25]. Being unsteady heat release rate and flame surface destruction important combustion noise generation mechanisms [26, 27], an impact of intrinsic thermodiffusive effects, via their action on flame surface, is probable, but has not yet been fully understood.

In this work, an investigation is conducted by means of numerical simulations and experimental measurements to study the noise generated by laminar hydrogen flames and examine the differences in noise generation when passing from conventional hydrocarbon fuels to full hydrogen. To this scope, lean hydrogen-air and stoichiometric methane-hydrogen-air laminar premixed M-shaped flames on a cylindrical bluff-body burner configuration at atmospheric conditions are considered. Most of the existing Computational Fluid Dynamics (CFD) models have been developed for reacting flows involving hydrocarbons and, therefore, may not be suitable to simulate pure hydrogen combustion [20]. Consequently, high-fidelity numerical simulations are here performed by adopting a fully-resolved flame approach, without implementing any combustion model. The reasonableness of the numerical results is assessed by comparison with experimental measurements, allowing also to validate the adopted computational approach. Flames of the two fuels are compared by considering two different configurations, keeping either the same flame height or the same ratio of bulk velocity over laminar burning velocity. In all cases, an acoustic perturbation is imposed to allow for an analysis of the flame motion and of the radiated sound field. The dynamics of flames for the different cases are analyzed first, together with the corresponding noise spectra. The common features and the discrepancies between the four cases are then discussed, in order to retrieve any similarities or differences in the noise generation process for the two fuels.

## 2. Methodology

Given the purpose of this study, a M-shaped laminar flame configuration has been considered. The study of laminar flames allows to highlight the impact, if any, of thermodiffusive effects in lean hydrogen flames, which would be masked by the interaction with turbulence in the case of non-laminar flows.

The stoichiometric methane-hydrogen flame cases, not affected by thermodiffusive effects, is considered as a reliable benchmark to isolate the peculiar features of lean hydrogen flames. For these flames, the hydrogen content is fixed at 24.0% of the total flame thermal power  $P_{th}$ . For pure hydrogen flames, instead, an equivalence ratio  $\phi = 0.50$  is adopted, so that a sub-unity Lewis number can be obtained, hence allowing for the preferential diffusion of hydrogen, without triggering thermodiffusive instabilities. With the chosen fuel-air mixtures' compositions, the same laminar burning velocity  $S_L = 60.0$  cm/s is kept for all configurations and fuels.

The mass flow rate  $\dot{m}$  has been adjusted for the four configurations, in order to obtain the desired value of flame height h or ratio of bulk velocity  $U_B$  over laminar burning velocity  $S_L$ . The main operating parameters for the four configurations are summarized in Table 1. Mass flow rate values are given in normal liters per minute (NLPM), with the normal temperature and pressure defined as  $T_n = 273.15 \text{ K}$  and  $p_n = 1$  atm.

Case No.	$P_{th}$ [kW]	H <sub>2</sub> Content [%]	φ [-]	m [NLPM]	$U_B$ [m/s]	$U_B/S_L$ [-]	h [mm]
1a	1.77	24.0	1.0	31.76	6.86	11.4	15.0
1b	1.21	100	0.50	38.32	8.27	13.8	15.0
2a	1.66	24.0	1.0	29.78	6.43	10.7	13.9
2b	0.940	100	0.50	29.84	6.44	10.7	12.2

Table 1 – Main operating parameters for the configurations considered in the study.

# 2.1 Experimental apparatus

The experimental results presented in this study are performed at the Institut de Mécanique des Fluides de Toulouse (IMFT) on the axisymmetric bluff-body burner shown in Figure 1. In this configuration, the burner has an annular outlet with an inner diameter d of 6 mm and an outer diameter D of 12 mm. The present set-up allows the study of M-shaped premixed laminar methane-hydrogen-air flames, as shown by the photographs in Figure 2 for Cases 1a and 1b.

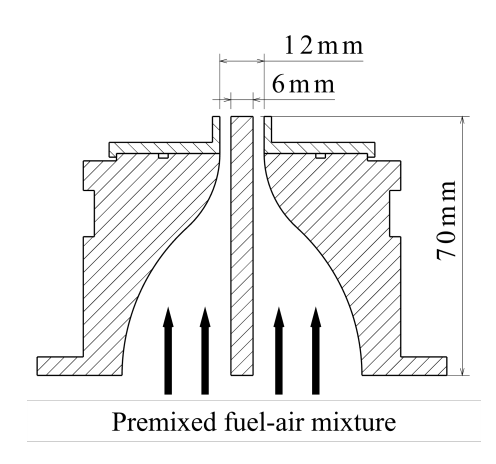


Figure 1 – Schematic representation of the bluff-body burner nozzle and outlet.

Two optical flow visualization methods are implemented to characterize the steady flame conditions. OH\* chemiluminescence is used to detect the flame structure and reaction zone while Particle Image Velocimetry (PIV) is performed to measure the velocity field of the reactive flow. The results of these diagnostics are used to validate the numerically predicted flow fields and thus improve the fidelity of the numerical simulations.

The OH\* chemiluminescence imaging technique makes use of a PI-MAX 2 intensified camera system from Princeton Instruments. The camera is equipped with a CERCO UV lens (100mm f/2.8) and an Edmund Optics bandpass filter (310 nm CWL and 10 nm FWHM) to record the OH\* flame luminescence. Flame images are recorded with an exposure time of 1.5 ms and an intensifier gain value of

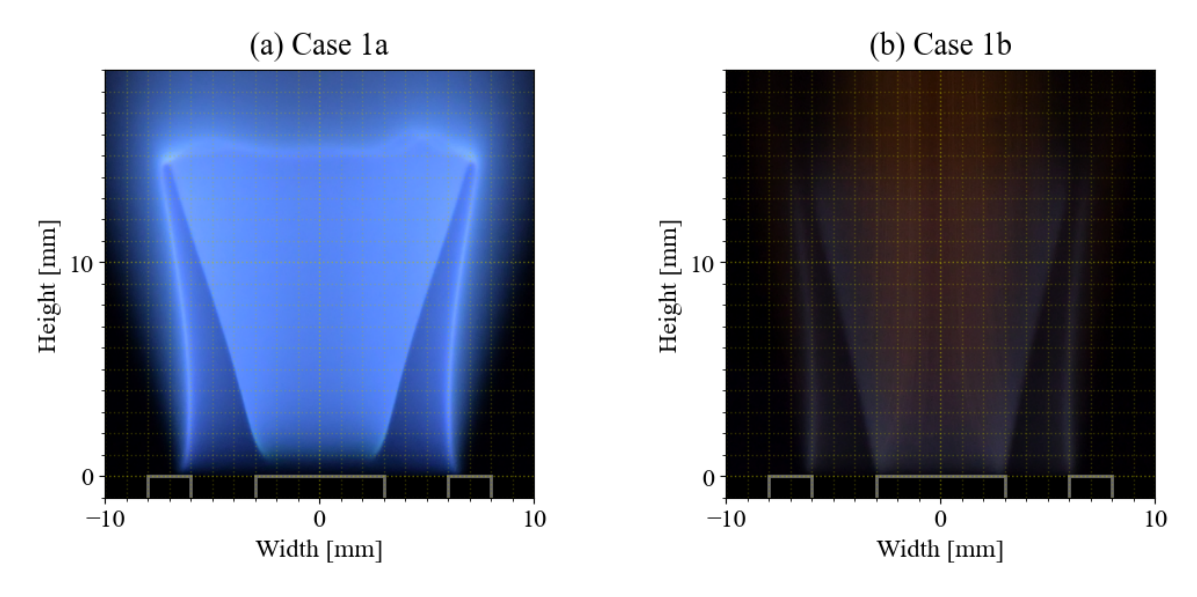


Figure 2 – Digital images for Cases 1a (a, left) and 1b (b, right) recorded using a Nikon D7500 camera with an exposure time of 100 ms for Case 1a and 1000 ms for Case 1b.

200. A deconvolution is performed using the inverse Abel transformation to view the flame structure in the axial plane of the burner.

The PIV measurements are achieved using two lamp pumped Nd:YAG lasers (Quantel CFR400) with a wavelength of 532 nm and a maximum beam energy of 300 mJ. From the laser beam, a laser sheet is generated using a combined LaVision sheet and collimator optics. The laser sheet has a thickness of approximately 0.5 mm in the center of the burner. The flow is seeded using solid particles with a sub-micron mean diameter and images of the illuminated particles are recorded using a LaVision Imager sCMOS camera. The image acquisition is controlled using the LaVision Davis software suite. The Davis software is then used for the processing of the particles images. A time filter subtraction is first performed, subsequently, the velocity vectors are calculated using a multi-pass approach with an initial window size of 64 pixels and a final window size of 16 pixels. A vector validation analysis is also conducted. This process results in a velocity vector field with data points every 0.113 mm.

The acoustic perturbation of the flames is achieved with a loudspeaker installed below the body of the burner. A Tektronix function generator (AFG1062) is used to create a sinusoidal waveform with a frequency of 228 Hz and a peak-to-peak voltage  $V_{pp}$  value chosen to bring about a velocity fluctuation of  $u_{rms}/\bar{u}=0.17$  at the burner outlet, as summarized in Table 2. The signal is conditioned by an amplifier set to -15 dB before being received by the loudspeaker. The velocity fluctuation is measured in equivalent air flow conditions using a hot-wire probe placed at 4.5 mm away from the burner axis and flush with the outlet.

Case No.	$V_{pp}$ [mV]	ū [m/s]	$u_{rms}$ [m/s]	$u_{rms}/\bar{u}$ [-]	
1a	230	8.78	1.50	0.17	
1b	279	10.4	1.77		
2a	215	8.30	1.40	0.17	
2b	215	8.33	1.41		

Table 2 – Velocity fluctuations and signal amplitudes for each operating condition.

The acoustic response of the flames is recorded by a Brüel & Kjær 1/4" free-field microphone (type 4954B) located 24 mm (i.e., 2D) above the burner outlet and at a radial distance of 72 mm (i.e., 6D) from the nozzle axis, as shown in Figure 3. The noise of each flame is measured by recording the signal for 10 s. Then, the raw microphone data is converted from volts to Pascals using the sensitivity value provided by the manufacturer (2.9 mV<sub>eff</sub> per Pa). Note that, this quantity was verified using a Brüel & Kjær sound level calibrator (type 4231).

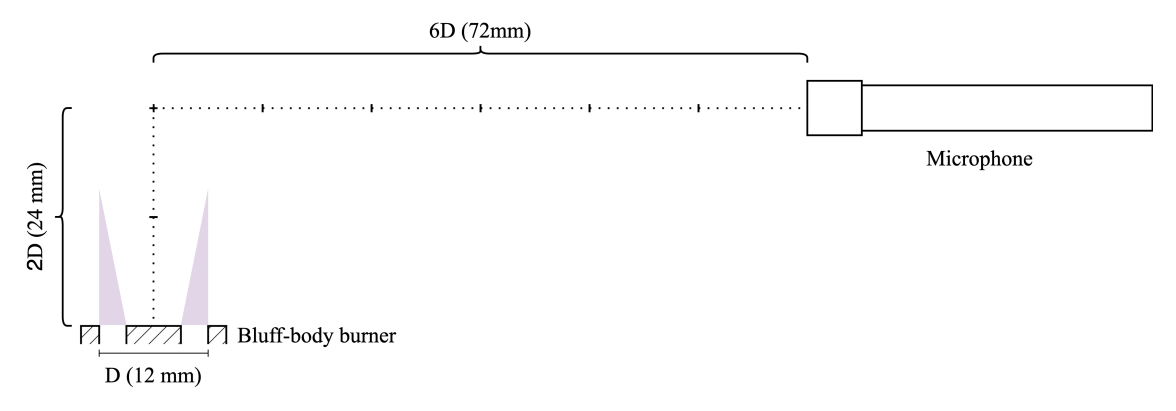


Figure 3 – Set-up of the microphone in the experimental apparatus.

# 2.2 Computational approach

High-fidelity numerical simulations of hydrogen and methane-hydrogen laminar flames are performed using the Navier-Stokes compressible solver AVBP (www.cerfacs.fr/avbp7x) developed at CERFACS (Toulouse, France), an explicit massively-parallel code solving the equations of conservation of mass, momentum, energy and species.

The computational domain adopted for all cases in this study is shown in Figure 4. The domain is hemispherical with diameter  $D_d = 200$  mm, a value deemed to be sufficiently large with respect to the dimension of the reactive region. The premixed air-fuel mixture is introduced in a section of the bluff-body burner 25 mm below the outlet. The latter is surrounded by an ambient air laminar coflow of inlet velocity  $u_{cf} = 0.5$  m/s.

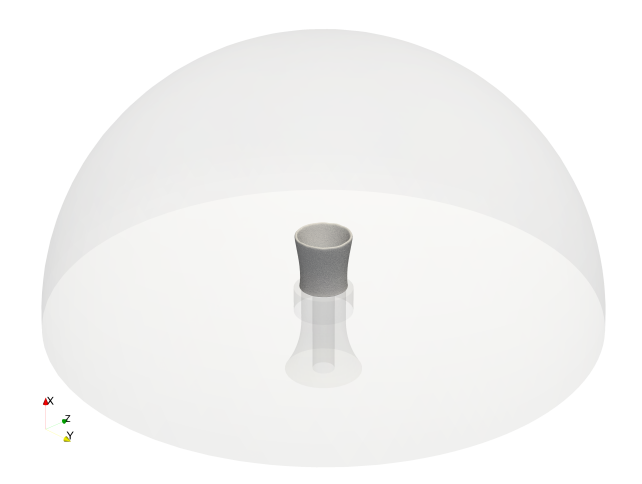


Figure 4 – Three-dimensional domain adopted for the numerical simulations.

The flame is fully resolved without implementing any combustion model. A sufficiently refined grid is thus implemented, with at least seven points in the flame front, whose thermal thickness  $\delta_L$ , evaluated according to the following definition [28]:

$$\delta_L = \frac{T_b - T_u}{\max |\nabla T|},\tag{1}$$

where  $T_u$  and  $T_b$  are the temperatures of the unburned and burned mixtures, is estimated by one dimensional unstretched premixed flame calculations performed with Cantera [29]. An unstructured mesh of tetrahedral elements, with a required minimum grid size of 40  $\mu$ m in the flame region, is sufficient to achieve the desired resolution.

To reduce the computational cost, a Lax—Wendroff finite-volume scheme is adopted for the discretization of convective terms [30], providing a second-order accuracy in both space and time. Diffusion terms are discretized with a second-order finite-element Galerkin scheme [31]. Inlet and outlet bound-

ary conditions are treated with the Navier–Stokes Characteristic Boundary Conditions (NSCBC) formulation [32]. The relaxation coefficient K at the outlet section is set to 1000, leading to a cutoff frequency  $f_c = K/(4\pi) \approx 80$  Hz [33]. Fresh gases are injected at the nozzle inlet with given composition, temperature and velocity, while static pressure is imposed at the outlet. A no-slip boundary condition is applied for the nozzle walls, with a heat resistance variable in the axial direction to allow for heat fluxes between the reacting mixture and the walls. The value of the heat resistance is estimated based on the experimentally recorded nozzle wall temperature. Once the flame is stabilized, an acoustic excitation of frequency  $f_a = 228$  Hz is imposed to the air-fuel mixture at the inlet to achieve the rms modulation level  $u_{rms}/\bar{u} = 0.17$  experimentally recorded on the center line at the nozzle outlet, with  $u_{rms}$  being the root mean square of the axial velocity fluctuation u', written as:

$$u'(t) = u(t) - \bar{u} = A\sin(2\pi f_a t),$$
 (2)

where t is the time and  $\bar{u}$  is the mean velocity.

The transport model is based on constant non-unity Lewis numbers for the species, with constant mixture Prandtl and species Schmidt numbers adopted to compute thermal and mass diffusivity terms. Dynamic viscosity  $\mu$  is approximated with a simple fitting power law.

The Analytically Reduced Chemistry (ARC) scheme CH4\_15\_256\_9\_AP [34], derived from the detailed CRECK mechanism [35] using ARCANE [36], is adopted for methane-hydrogen flames. The scheme consists of 15 transported species, 256 irreversible reactions and 9 quasi-steady state species. For hydrogen flames, the San Diego mechanism [37], comprising 9 species and 21 reactions, is adopted. To allow for a proper comparison with experimental CLI images, the OH\* distribution is numerically computed by considering the sub-scheme proposed by Kathrotia et al. [38, 39] to describe OH\* formation and consumption. Indeed, it has been observed that, for premixed hydrogen-air flames, the correlation between OH\* and heat release rate fails, making it not possible to directly compare the sole numerically computed heat release rate distributions with the experimentally recorded OH\* chemiluminescence images [40]. The OH\* sub-scheme is simply added to the main reaction scheme as its impact on the ground species' concentrations is negligible [41], and quasi-steady state behavior is assumed for this radical. A detailed description of chemical kinetics is thus adopted for both fuel mixtures. Indeed, although global reaction mechanisms have been developed in the literature both for hydrogen (e.g., [42]) and methane-hydrogen (e.g., [43]) flames, the impact of a simplified kinetics description on the computed noise radiation is unclear and needs further assessment.

## 3. Results

To assess the adequacy of the adopted numerical set-up, results of stabilized hydrogen and methanehydrogen flames are validated with experimental measurements. Only Cases 1a and 1b of Table 1 are here considered.

First, the numerically computed axial velocity fields for the two flames are compared with the experimental PIV data at several distances h from the burner outlet in Figure 5. An overall good agreement is observed between numerical and experimental results, especially at h = 0.5 mm and between the flame fronts, which are marked by the dashed black lines. A slightly poorer agreement is found in the central burned gas region where, however, the results of the PIV measurements present a larger uncertainty due to seeding issues in this area, as shown by the orange error bars in the figure. Indeed, these are affected by the wake of the bluff-body, whose position is marked by the shaded gray zone in the figure.

Figure 6 compares the experimentally measured and numerically predicted spatial distributions of OH\* for methane-hydrogen (Case 1a) and hydrogen (Case 1b) flames. Overall, the numerical simulations are able to fairly well reproduce the flame shape, as well as the position of the flame leading edge and the flame height. Nevertheless, in all cases the numerically predicted distributions further extend above the burner with respect to the experimental images. This may be due to the lifting of the flame near the bluff-body top wall, which is more accentuated with respect to the experimentally observed one. Overall, the results of Figures 5 and 6 sustain the adequacy of the numerical set-up adopted in this study.

The numerical results for the acoustically excited flames are reported in Figure 7, where the temporal profiles of the fluctuations of pressure p' and heat release rate (HRR)  $\dot{Q}'$  for the four cases considered

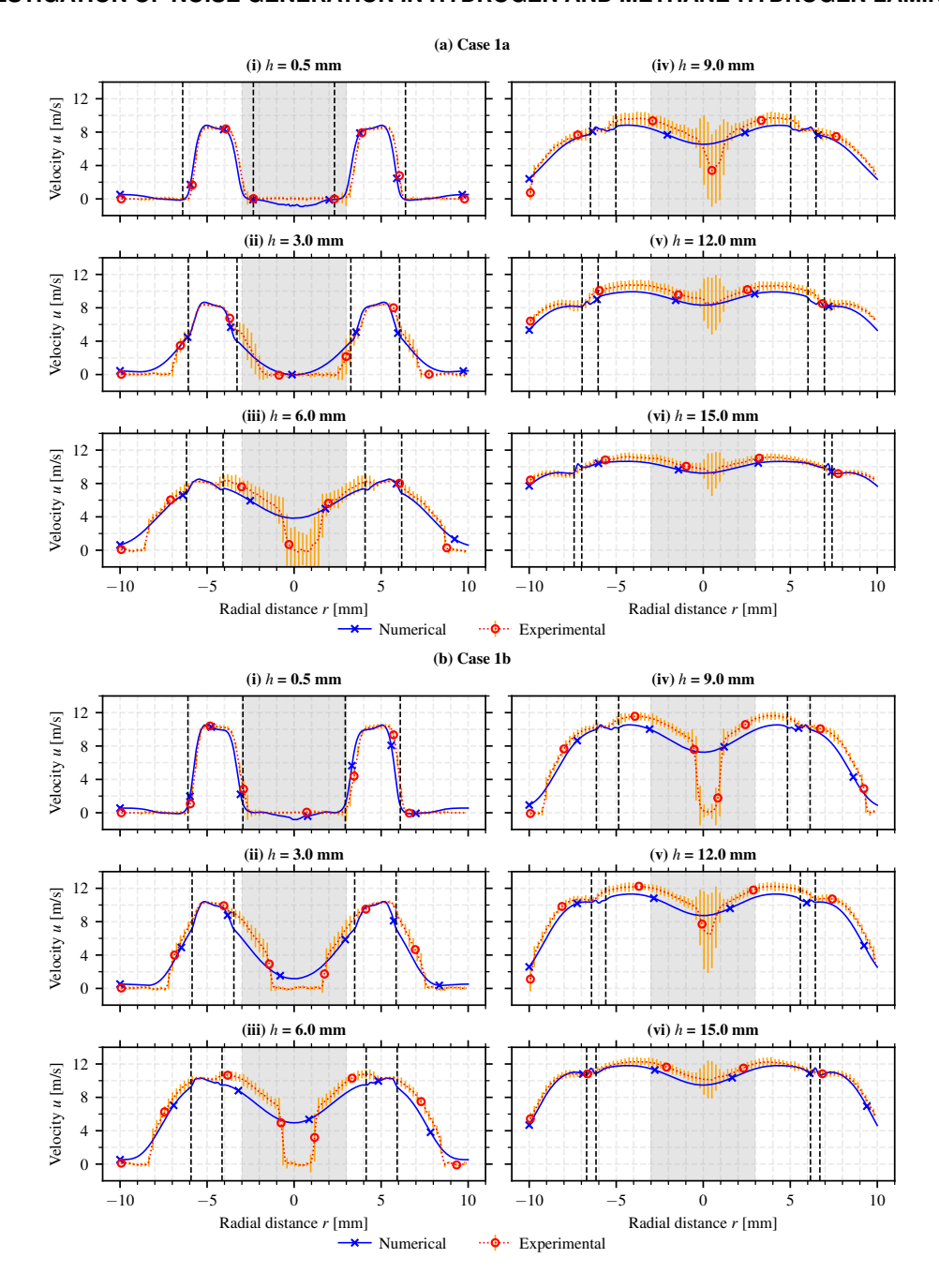


Figure 5 – Comparison of radial profiles of axial velocity *u* computed numerically (blue) and recorded experimentally via PIV (red) for Cases 1a (a, top) and 1b (b, bottom) at different heights *h* from the burner outlet. For the experimental measurements, the standard deviation of the measurements is reported in orange. The vertical dashed black correspond to the peaks of HRR and highlight the reactive region. The shaded grey zone identifies the radial position of the bluff-body.

in the study are shown. All temporal signals are synchronized with respect to the velocity signals recorded at the mean radius of the burner in correspondence of the outlet section, reported in Figure 8, which are periodic with period  $T=1/f_a$ .

It can be observed that the HRR fluctuations (normalized by the time average value) are comparable between the two fuel mixtures. Nevertheless, a difference in the corresponding pressure fluctuation profiles is observed, with the methane-hydrogen flames showing a larger fluctuation than pure hydrogen ones. Furthermore, for the methane-hydrogen flames, the pressure fluctuation temporal profile shows a local peak at time  $t \approx 0.7kT$  (with  $k \in \mathbb{Z}$ ). This is associated with a localized change of slope in the corresponding HRR fluctuation profile at the same time instant.

Observing the snapshots of the HRR distribution at different time instants during the cyclic modulation

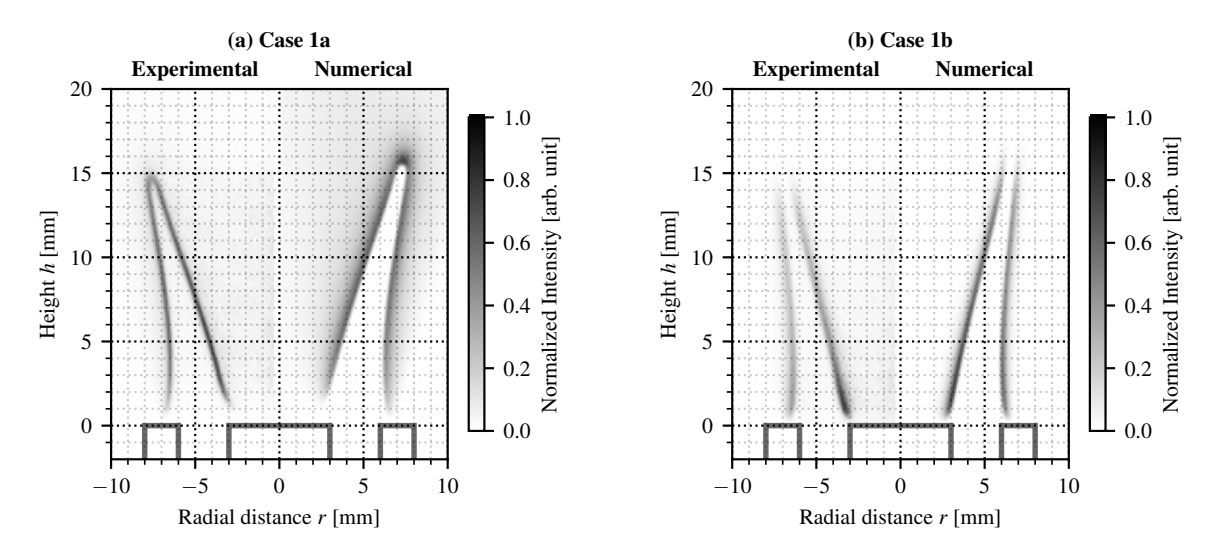


Figure 6 – Comparison of normalized distributions of numerically computed OH\* concentration and experimentally recorded Abel-deconvoluted OH\* chemiluminescence images for Cases 1a (a, left) and 1b (b, right). The position of the bluff-body burner is added for reference.

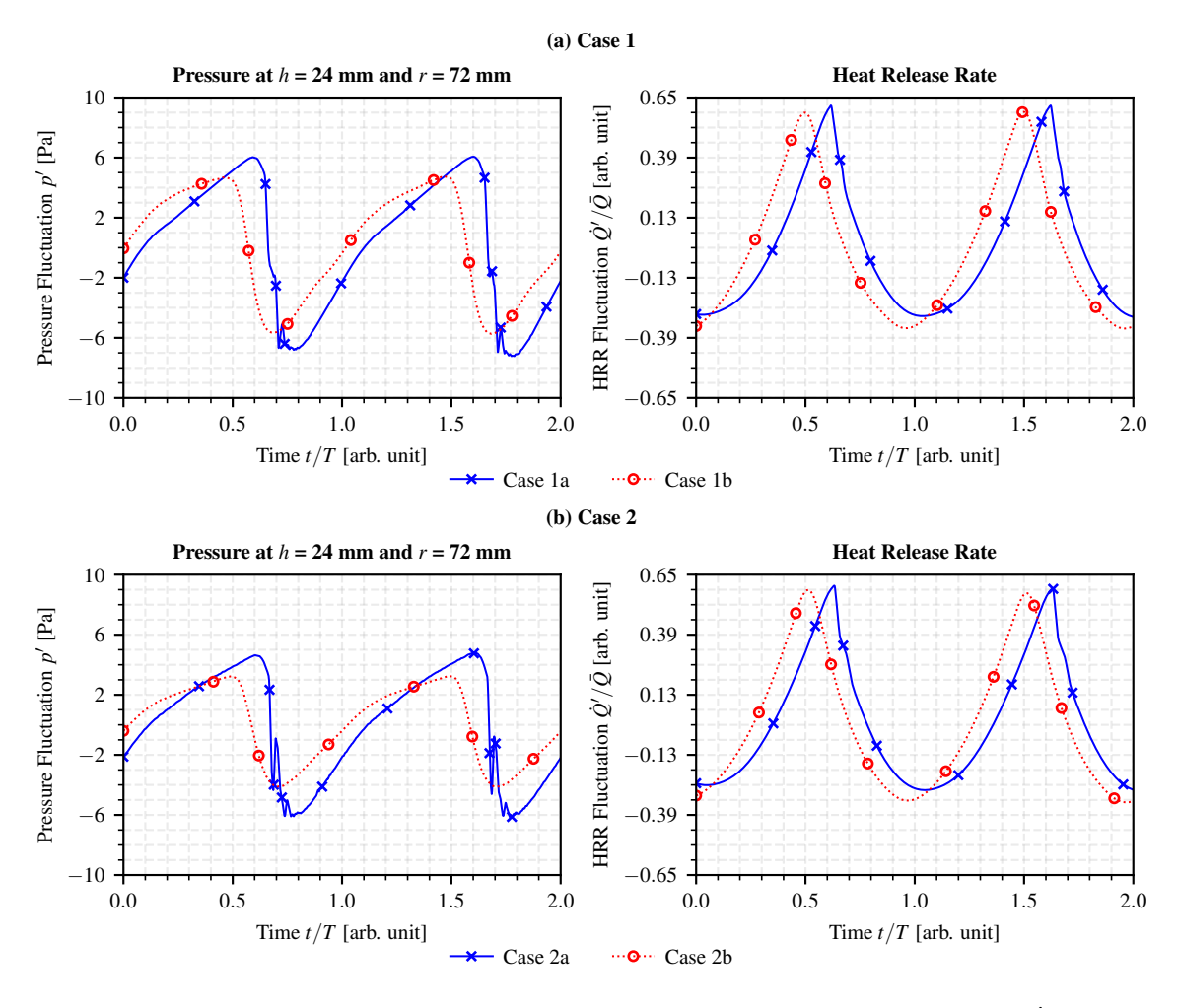


Figure 7 – Temporal profiles of the fluctuations of pressure p' and heat release rate  $\dot{Q}'$  (normalized by the time average  $\bar{Q}$ ) for Cases 1 (a, top) and Cases 2 (b, bottom).

of the flow for Cases 1a and 1b reported in Figure 9, this trend of the pressure and HRR profiles for Cases 1a and 2a can be related to the detachment of a pocket of reactants from the elongated flame filament, a phenomenon denominated "pinch-off" in [17] and observed to be a strong source of sound [26]. From Figure 9, it can also be observed that the pure hydrogen flame, which presents an

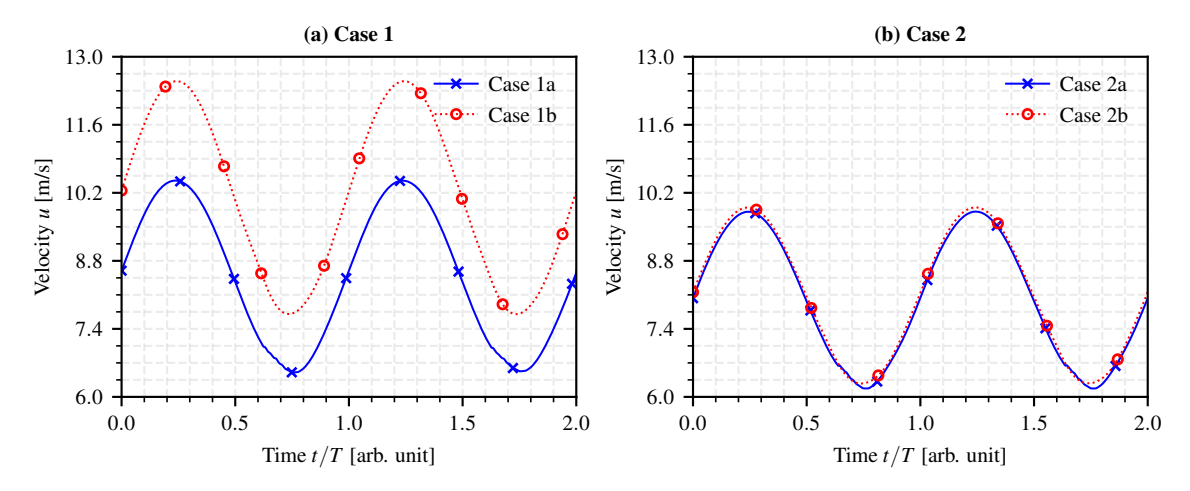


Figure 8 – Temporal signals of velocity *u* recorded at the mean radius of the burner in correspondence of the outlet section for Cases 1 (a, left) and Cases 2 (b, right).

open tip in the stabilized, non perturbed configuration (see Figure 6), presents a weaker flame-flame interaction, with the inner and outer branches of the M-shaped flame remaining separated, without any appreciable mutual annihilation. As flame surface reduction is considered the main combustion noise generation mechanism [12, 27], the less accentuated variation in the flame surface area can explain the weaker pressure fluctuation observed for hydrogen flames.

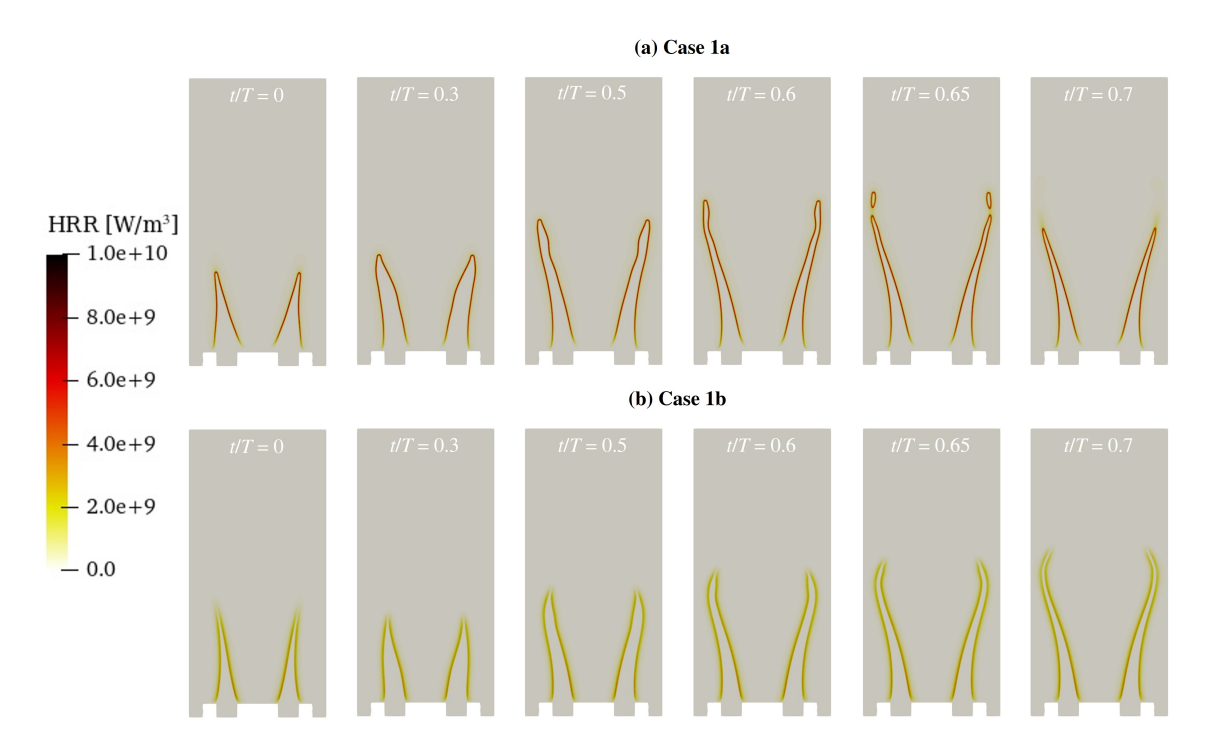


Figure 9 – Snapshots of the cyclic flame motion (denoted by the HRR field) for Cases 1a (a, top) and 1b (b, bottom) taken in a transversal section at different time instants.

From the temporal profiles in Figure 7, as well as from the snapshots in Figure 9, it can also be observed that methane-hydrogen flames present a time delay in their response with respect to the velocity signal at nozzle outlet, while the response of the hydrogen flame is more synchronized with the acoustic forcing, with the peak values of p' and  $\dot{Q}'$  located almost at the same time instant of the corresponding velocity signal. This suggests a strong difference between the two fuels in the process of energy transfer between outlet velocity fluctuations and sound radiation.

Nevertheless, the corresponding spectra do not seem to be sensibly affected. In this work, the Power Spectral Density (PSD) is estimated by using the Welch's method [44]. Signals are windowed by the

means of Tukey windows [45] with shape parameter  $\alpha=0.15$  and length corresponding to 12T. Figure 10 shows the PSD distribution in the frequency domain of HRR fluctuation  $P_{\hat{Q}'\hat{Q}'}$ . No significant differences can be observed among the four operating conditions in the low-frequency region (below 1000 Hz), especially for the peak value, which is located in correspondence of the forcing frequency  $f_a=228$  Hz. Major differences between the two fuel mixtures can be observed instead at higher frequencies, where the hydrogen flames present lower peak values with respect to methane-hydrogen ones. This difference may be related to the presence, in the latter, of the aforementioned flame annihilation phenomena.

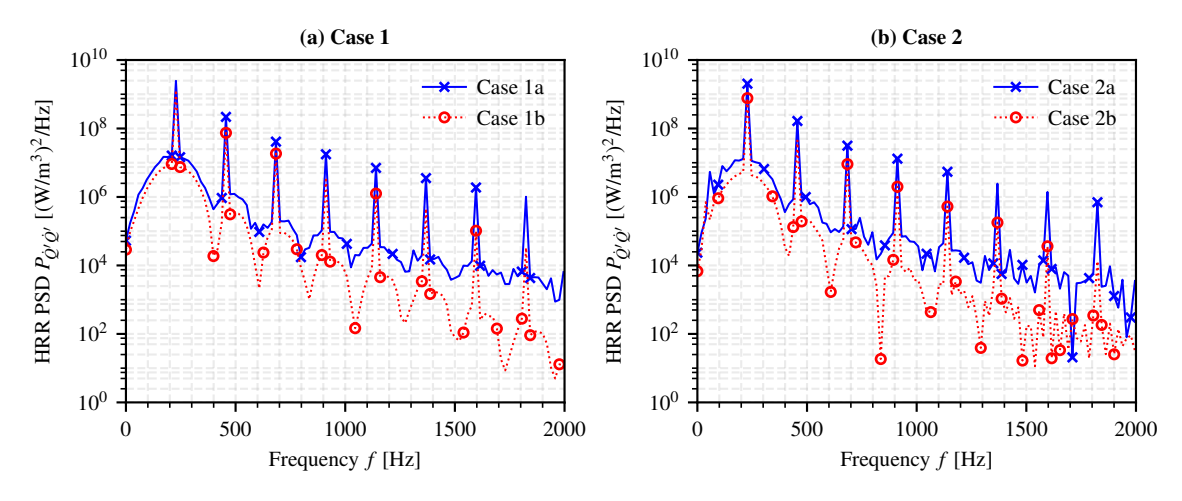


Figure 10 – Power spectral density of HRR fluctuation  $P_{\hat{Q}'\hat{Q}'}$  for Cases 1 (a, left) and Cases 2 (b, right) in logarithmic scale.

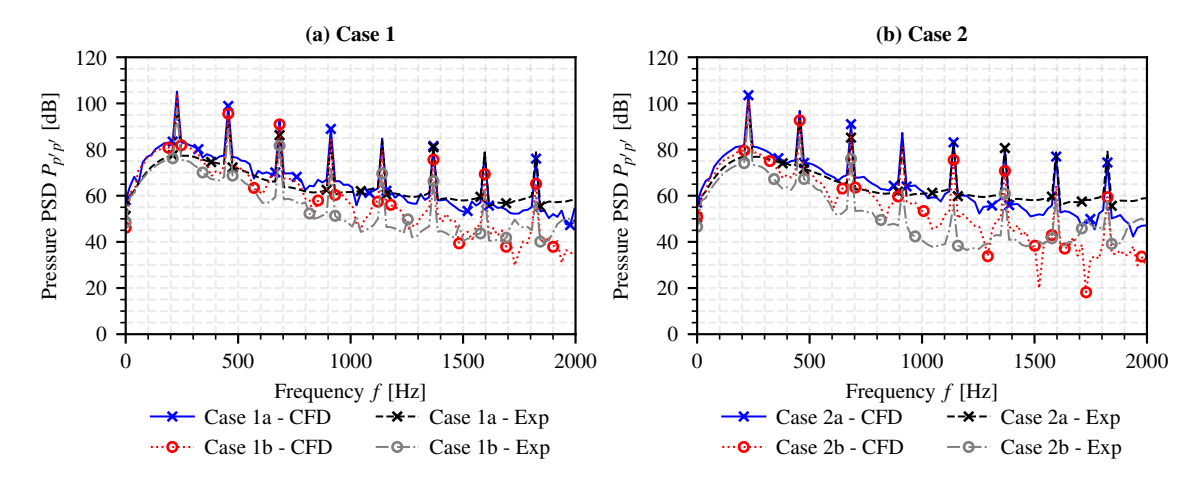


Figure 11 – Power spectral density of pressure fluctuation  $P_{p'p'}$  for Cases 1 (a, left) and Cases 2 (b, right). Comparison between numerical (CFD) and experimental (Exp) results.

As for the noise spectrum, Figure 11 shows the PSD distribution of pressure fluctuation, computed in dB according to the following definition:

$$PSD \left[ \mathsf{dB} \right] = 10 \log_{10} \left( \frac{P_{p'p'} \left[ \mathsf{Pa}^2 / \mathsf{Hz} \right] \Delta f}{p_{ref}^2} \right), \tag{3}$$

where  $\Delta f$  is the spectral resolution and  $p_{ref}=2\times10^{-5}$  Pa is a reference acoustic pressure [12]. The numerical results are here compared with the experimentally recorded noise spectrum. Focusing on the numerical results first, it can be observed that, despite the differences in the temporal profiles of p', the value at 228 Hz is almost the same for all cases. Indeed, the Sound Pressure Level SPL, defined as

$$SPL [dB] = 20\log_{10}\left(\frac{p_{rms}}{p_{ref}}\right), \tag{4}$$

is equal, respectively, to 106.7 dB for Case 1a, 105.2 dB for Case 1b, 105.0 dB for Case 2a, and 102.2 dB for Case 2b. It can therefore be deduced that, despite the absence of visible flame annihilation phenomena, the hydrogen flame is able to produce a comparable noise level for both the operating conditions. The other peak frequencies are located at harmonics of this fundamental frequency. At least for the first six peaks, a linear trend can be observed for the corresponding amplitudes, hence indicating a power law dependency of  $P_{p'p'}$  with respect to frequency, which is in agreement with the literature on the subject [12]. For the hydrogen flames, a more rapid decay is observed with respect to methane-hydrogen flames.

As for the experimental results, it can be observed for all cases that the recorded values are slightly lower than the numerical ones. The amplitude of the peak at 228 Hz is approximately 5 dB lower than the numerical value, with the SPL values now equal, respectively, to 101.2 dB for Case 1a, 98.7 dB for Case 1b, 100.6 dB for Case 2a, and 96.4 dB for Case 2b. Nevertheless, a reasonable correspondence is found between experimental and numerical results in the trends, sustaining the capability of the numerical set-up to properly capture the features of this system.

# 4. Conclusion and Perspectives

The generation of noise in laminar hydrogen and methane-hydrogen flames has been investigated experimentally and numerically by considering acoustically excited M-shaped flames over a bluff-body burner at either the same flame length or the same ratio of bulk velocity over laminar burning velocity. The comparison of experimental and numerical results for both stable and forced flames has shown the capability of the numerical set-up to adequately reproduce the main features of the flame. In all cases, it has been observed that methane-hydrogen flames produce more accentuated pressure fluctuations than pure hydrogen ones. This can be related to the presence, in acoustically excited methane-hydrogen flames, of more pronounced flame-flame interactions which trigger "pinch-off" phenomena. These cause the annihilation of the flame surface, a well-known mechanism of sound generation. In the pure hydrogen flames, instead, due to the open-tip configuration of the stable flame, flame-flame interactions are less accentuated at the flame tip for the same excitation frequency, hampering the flame annihilation mechanism and leading to a reduced noise emission.

Nevertheless, the comparison of noise spectra has shown that the differences in terms of Power Spectral Density at the peak frequency, as well as of Sound Pressure Level, between the two fuel mixtures are quite limited. Therefore, despite the absence of abrupt flame surface destruction phenomena as the "pinch-off" observed in methane-hydrogen flames, pure hydrogen flames present a comparable emitted noise level. The main discrepancies are found in the amplitude of the harmonics, with hydrogen flames showing a faster decay of the peak amplitudes for increasing frequencies.

In future work, the approach and methodology presented in this work will be extended to other excitation frequencies and operating conditions. The impact of thermodiffusive instabilities in hydrogen flames will be also investigated, by considering a leaner fuel-air mixture, in order to determine under which states acoustically excited laminar hydrogen flames are capable to emit more noise than methane-hydrogen ones. The considerations made for laminar flames will allow to better understand the impact of flame-turbulence interaction on direct combustion noise generation in turbulent reacting flows, which will be the subject of subsequent studies.

## 5. Acknowledgments

The authors would like to acknowledge CERFACS for the grant to use the AVBP code, and the CINECA award under the ISCRA initiative (Class C Project INTONATE and Class B Project SONIC-H2), for the availability of high performance computing resources and support. Part of the numerical simulations was performed on the Luxembourg national supercomputer MeluXina. The authors gratefully acknowledge the LuxProvide teams for their expert support, and EuroHPC JU for awarding the related high performance computing resources under the Project PROMETH2EUS. This work has been supported under the National Recovery and Resilience Plan (NRRP), Mission 4 Component 2 Investment 1.3 - Call for tender No. 1561 of October 11, 2022 of the Italian Ministry of University and Research, funded by the European Union - NextGenerationEU [Project code PE0000021, Concession Decree No. 1561 of October 11, 2022 adopted by the Italian Ministry of University and Research, CUP: D93C22000900001, Project title "Network 4 Energy Sustainable Transition – NEST"], and the

grant ANR-AAPG-2022 TOHREAU of the French National Research Agency. This project received funding from European Union Horizon ERC SELECT-H (Grant 101097984).

# 6. Contact Author Email Address

Francesco G. Schiavone: f.schiavone11@phd.poliba.it

# 7. Copyright Statement

The authors confirm that they, and/or their company or organization, hold copyright on all of the original material included in this paper. The authors also confirm that they have obtained permission, from the copyright holder of any third party material included in this paper, to publish it as part of their paper. The authors confirm that they give permission, or have obtained permission from the copyright holder of this paper, for the publication and distribution of this paper as part of the ICAS proceedings or as individual off-prints from the proceedings.

## References

- [1] S. Gössling and A. Humpe. Net-zero aviation: Time for a new business model? *Journal of Air Transport Management*, 107:102353, 2023.
- [2] International Air Transport Association. Global Outlook for Air Transport A local sweet spot, December 2023. IATA Economics Report.
- [3] C. Bergero, G. Gosnell, D. Gielen, S. Kang, M. Bazilian, and S.J. Davis. Pathways to net-zero emissions from aviation. *Nature Sustainability*, 6(4):404–414, 2023.
- [4] D. Cecere, E. Giacomazzi, and A. Ingenito. A review on hydrogen industrial aerospace applications. *International Journal of Hydrogen Energy*, 39(20):10731–10747, 2014.
- [5] T. Capurso, M. Stefanizzi, M. Torresi, and S.M. Camporeale. Perspective of the role of hydrogen in the 21st century energy transition. *Energy Conversion and Management*, 251:114898, 2022.
- [6] J.L. Sloop. *Liquid hydrogen as a propulsion fuel, 1945-1959*, volume 4404. Scientific and Technical Information Office, National Aeronautics and Space Administration, 1978.
- [7] V. Sosounov and V. Orlov. Experimental turbofan using liquid hydrogen and liquid natural gas as fuel. In *26th Joint Propulsion Conference*, page 2421, 1990.
- [8] M. Stefanizzi, T. Capurso, G. Filomeno, M. Torresi, and G. Pascazio. Recent combustion strategies in gas turbines for propulsion and power generation toward a zero-emissions future: fuels, burners, and combustion techniques. *Energies*, 14(20):6694, 2021.
- [9] W.R. Graham, C.A. Hall, and M.V. Morales. The potential of future aircraft technology for noise and pollutant emissions reduction. *Transport Policy*, 34:36–51, 2014.
- [10] M. Ihme. Combustion and engine-core noise. Annual Review of Fluid Mechanics, 49:277-310, 2017.
- [11] A.P. Dowling and Y. Mahmoudi. Combustion noise. *Proceedings of the Combustion Institute*, 35(1):65–100, 2015.
- [12] S. Candel, D. Durox, S. Ducruix, A.-L. Birbaud, N. Noiray, and T. Schuller. Flame dynamics and combustion noise: progress and challenges. *International Journal of Aeroacoustics*, 8(1):1–56, 2009.
- [13] S.L. Bragg. Combustion noise. *Journal of the Institute of Fuel*, 36(1):12–16, 1963.
- [14] W.C. Strahle. Combustion noise. *Progress in Energy and Combustion Science*, 4(3):157–176, 1978.
- [15] H.A. Hassan. Scaling of combustion-generated noise. *Journal of Fluid Mechanics*, 66(3):445–453, 1974.
- [16] F.E. Marble and S.M. Candel. Acoustic disturbance from gas non-uniformities convected through a nozzle. *Journal of Sound and Vibration*, 55(2):225–243, 1977.
- [17] M. Talei, M.J. Brear, and E.R. Hawkes. A comparative study of sound generation by laminar, combusting and non-combusting jet flows. *Theoretical and Computational Fluid Dynamics*, 28:385–408, 2014.
- [18] C.K.W. Tam, F. Bake, L.S. Hultgren, and T. Poinsot. Combustion noise: modeling and prediction. *CEAS Aeronautical Journal*, 10:101–122, 2019.
- [19] T.L. Howarth, E.F. Hunt, and A.J. Aspden. Thermodiffusively-unstable lean premixed hydrogen flames: Phenomenology, empirical modelling, and thermal leading points. *Combustion and Flame*, 253:112811, 2023.
- [20] V. Coulon, J. Gaucherand, V. Xing, D. Laera, C. Lapeyre, and T. Poinsot. Direct numerical simulations of methane, ammonia-hydrogen and hydrogen turbulent premixed flames. *Combustion and Flame*, 256:112933, 2023.
- [21] E. Æsøy, J.G. Aguilar, S. Wiseman, M.R. Bothien, N.A. Worth, and J.R. Dawson. Scaling and prediction of transfer functions in lean premixed H2/CH4-flames. *Combustion and Flame*, 215:269–282, 2020.

- [22] T. Lee and K.T. Kim. High-frequency transverse combustion instabilities of lean-premixed multislit hydrogen-air flames. *Combustion and Flame*, 238:111899, 2022.
- [23] T. Schuller, D. Durox, and S. Candel. A unified model for the prediction of laminar flame transfer functions: comparisons between conical and v-flame dynamics. *Combustion and Flame*, 134(1-2):21–34, 2003.
- [24] R. Rajaram and T. Lieuwen. Acoustic radiation from turbulent premixed flames. *Journal of Fluid Mechanics*, 637:357–385, 2009.
- [25] M.S. Wu, S. Kwon, J.F. Driscoll, and G.M. Faeth. Preferential diffusion effects on the surface structure of turbulent premixed hydrogen/air flames. *Combustion Science and Technology*, 78(1-3):69–96, 1991.
- [26] T. Schuller, D. Durox, and S. Candel. Self-induced combustion oscillations of laminar premixed flames stabilized on annular burners. *Combustion and Flame*, 135(4):525–537, 2003.
- [27] S. Candel, D. Durox, and T. Schuller. Flame interactions as a source of noise and combustion instabilities. In *10th AIAA/CEAS Aeroacoustics Conference*, page 2928, 2004.
- [28] T. Poinsot and D. Veynante. Theoretical and numerical combustion. RT Edwards, Inc., 2005.
- [29] D.G. Goodwin, H.K. Moffat, and R.L. Speth. Cantera: An Object-oriented Software Toolkit for Chemical Kinetics, Thermodynamics, and Transport Processes. https://www.cantera.org, 2017. Version 2.3.0.
- [30] P. Lax and B. Wendroff. Systems of conservation laws. *Communications on Pure and Applied Mathematics*, 13:217, 1960.
- [31] O. Colin and M. Rudgyard. Development of High-Order Taylor–Galerkin Schemes for LES. *Journal of Computational Physics*, 162(2):338–371, 2000.
- [32] T.J. Poinsot and S.K. Lele. Boundary conditions for direct simulations of compressible viscous flows. *Journal of Computational Physics*, 101(1):104–129, 1992.
- [33] L. Selle, F. Nicoud, and T. Poinsot. Actual impedance of nonreflecting boundary conditions: Implications for computation of resonators. *AIAA Journal*, 42(5):958–964, 2004.
- [34] A. Pestre. *Numerical simulations of aeronautical engine ignitions under realistic high altitude conditions*. PhD thesis, Institut National Polytechnique de Toulouse INPT, 2023.
- [35] E. Ranzi, A. Frassoldati, A. Stagni, M. Pelucchi, A. Cuoci, and T. Faravelli. Reduced kinetic schemes of complex reaction systems: fossil and biomass-derived transportation fuels. *International Journal of Chemical Kinetics*, 46(9):512–542, 2014.
- [36] Q. Cazères, P. Pepiot, E. Riber, and B. Cuenot. A fully automatic procedure for the analytical reduction of chemical kinetics mechanisms for computational fluid dynamics applications. *Fuel*, 303:121247, 2021.
- [37] P. Saxena and F.A. Williams. Testing a small detailed chemical-kinetic mechanism for the combustion of hydrogen and carbon monoxide. *Combustion and Flame*, 145(1-2):316–323, 2006.
- [38] T. Kathrotia, M. Fikri, M. Bozkurt, M. Hartmann, U. Riedel, and C. Schulz. Study of the H+O+M reaction forming OH: Kinetics of OH\* chemiluminescence in hydrogen combustion systems. *Combustion and Flame*, 157(7):1261–1273, 2010.
- [39] T. Kathrotia, U. Riedel, A. Seipel, K. Moshammer, and A. Brockhinke. Experimental and numerical study of chemiluminescent species in low-pressure flames. *Applied Physics B*, 107(3):571–584, 2012.
- [40] F.G. Schiavone, A. Aniello, E. Riber, T. Schuller, and D. Laera. On the adequacy of OH\* as heat release marker for hydrogen-air flames. *Proceedings of the Combustion Institute*, Manuscript accepted for publication.
- [41] J. Graña-Otero and S. Mahmoudi. Excited OH kinetics and distribution in H2 premixed flames. *Fuel*, 255:115750, 2019.
- [42] F.G. Schiavone, N. Detomaso, M. Torresi, and D. Laera. An Arrhenius-based one-step reaction mechanism for hydrogen-air flames simulations in an extended range of operating conditions. *International Journal of Hydrogen Energy*, 57:1229–1243, 2024.
- [43] H.Y. Kim and N.I. Kim. Optimized global reaction mechanisms for H2, CO, CH4, and their mixtures. *International Journal of Hydrogen Energy*, 48(62):24101–24112, 2023.
- [44] P. Welch. The use of fast Fourier transform for the estimation of power spectra: A method based on time averaging over short, modified periodograms. *IEEE Transactions on audio and electroacoustics*, 15(2):70–73, 1967.
- [45] F.J. Harris. On the use of windows for harmonic analysis with the discrete Fourier transform. *Proceedings of the IEEE*, 66(1):51–83, 1978.